SEISMO-ACOUSTIC DETERMINATION OF THE SHEAR-WAVE SPEED OF SURFICIAL CLAY AND SILT SEDIMENTS ON THE SCOTIAN SHELF

John C. Osler[*] and David M. F. Chapman

Defence Research Establishment Atlantic
P.O. Box 1012, Dartmouth
Nova Scotia, B2Y 3Z7, Canada
email: dave.chapman@drea.dnd.ca

ABSTRACT

The Defence Research Establishment Atlantic has determined the shear-wave speed profile of the unconsolidated surficial clay and silt sediments at two locations on the Scotian Shelf—the shallow water continental margin of Nova Scotia, Canada. An ocean bottom seismometer detected the passage of interface waves which were generated by detonating small explosives on the seabed. Profiles of shear speed as a function of depth were determined by repetitive forward modelling of the measured dispersion of the interface waves. The shear speed of the approximately 25 to 40 m thick Quaternary succession of clay and silt ranges from approximately 10 m/s at the seabed to 120 m/s at 40 m depth. The shear speed profiles are consistent with a power-law relationship of the form $c_s(z) = c_0 z^\nu$, with ν in the range 0.60-0.65 and c_0 in the range 16-22 m/s re 1 m. The shear speeds encountered in this study are among the lowest that have been reported for any marine sediment in the literature, while the strength of the gradient, ν, is approximately twice that which is typically observed.

SOMMAIRE

Le Centre de recherches pour la défense Atlantique a determiné le profil de vitesse des ondes de cisaillement dans des sédiments superficiel meuble d'argile et de limon à deux emplacements sur le plateau continentale écossais (les eaux continentales peu profondes au bord de la Nouvelle-Ecosse, Canada). Un sismomètre de fond d'océan détecte le passage d'ondes d'interface qui sont produites en détonant de petits explosifs sur le fond marin. Les profils de vitesse de cisaillement en fonction de la profondeur ont été déterminé en modélisant de façon répétitive la dispersion des ondes d'interface qui ont été mesurée. Dans la succession de couche d'argile et de limon du quaternaire qui est d'environ 25 à 40 m de profondeur, la vitesse des ondes de cisaillement varie entre approximativement 10 m/s sur le fond marin à 120 m/s à 40 m de profondeur. Les profils de vitesse de cisaillement sont consistants avec une relation de puissance de la forme $c_s(z) = c_0 z^\nu$ où ν varie entre 0.60 et 0.65, et c_0 varie entre 16 et 22 m/s re 1 m. Les vitesses de cisaillement obtenues dans cette étude sont parmies les plus basses qui ont été rapporté pour un sédiment marin, tandis que l'intensité du gradient, ν, est approximativement le double de ce qui est typiquement observé.

1. INTRODUCTION

The shear-wave speed in unconsolidated surficial marine sediments and its dependence on depth is a physical property which is of interest to a broad community of researchers including acousticians, marine geophysicists, and geotechnical engineers. The shear speed of a sediment is a function of its shear strength—a property which is relevant

to problems concerning seabed stability, such as earthquake risk assessment and the construction of offshore structures. For acousticians, conversion of compressional waves in the water to shear waves in the seabed has been identified as a significant propagation loss mechanism, particularly at lower frequencies and in shallow water [*e.g.* Akal, 1980]. In some seabeds, the shear speed profile dominates over other parameters (such as shear-wave attenuation, compressional-wave speed and attenuation, and density) in controlling propagation loss [*e.g.* Dosso and Brooke, 1995].

---

[*] Current address: SACLANT Undersea Research Centre, Viale San Bartolomeo 400, 10138 San Bartolomeo (SP), Italy.

DREA's interest in shear wave effects in ocean acoustics is motivated by a desire to understand the influence of the seabed on the low-frequency performance of passive sonar systems, which endeavour to detect, locate, and classify submarines using the sounds that these vessels radiate naturally as a consequence of operating and transiting underwater [Chapman *et al.*, 1992]. Of secondary interest is the relation of shear speed to sediment stiffness and the ease with which anti-ship mines might be buried in Canadian shallow waters.

Direct measurements of shear-wave speed may be conducted *in situ* using probes (*e.g.* shear wave transducers or cone penetrometers) inserted into the sediment, in the laboratory by inserting probes into cores, or using vibrational techniques such as the resonant column test [Bennell and Smith, 1991]. The *in situ* measurements are typically limited in depth [*e.g.* Muir *et al.*, 1991], are time consuming, and often require support from divers or submersibles [*e.g.* Hamilton *et al.*, 1970]. Laboratory measurements have consistently shown lower values than *in situ* measurements [*e.g.* Richardson *et al.*, 1989; Stoll *et al.*, 1988] due to disturbance during collection, transportation, storage, and mechanical manipulation and reduction in confining pressure. Both methods, in particular the laboratory techniques using probes, make measurements at frequencies which are higher than those at which conversion to shear waves is identified as a significant propagation loss mechanism in field experiments.

Indirect measurements can use impulsive sources located at or near the seabed to generate interface waves on the water-sediment boundary and shear body waves within the sediment. These are detected by receivers located on or below the seabed. Sources include explosive charges and compressed air guns (summarized in Stoll *et al.* [1991] and Dodds [1995]), which may be configured into "shear-wave sleds" [Ewing *et al.*, 1992; Davis *et al.*, 1989] and torsional sources which generate horizontally polarized shear waves (SH) [Stoll *et al.*, 1994]. Receivers are typically geophone sensors although hydrophones located in proximity to the seabed are capable of detecting the compressional component of an interface wave. The underlying shear speed profile may be determined through a process of forward modelling to model the dispersion characteristics of the interface wave [*e.g.* Dosso and Brooke, 1995; Ali and Bibee, 1993] or in a more automated fashion through an inversion algorithm [*e.g.* Stoll *et al.* 1994; Caiti *et al.*, 1993]. The advantages of the indirect techniques are that they sample a larger volume, use more realistic frequencies, do not disturb the structural integrity of the sediment, and can resolve the shear speed to a greater depth.

The experiment described in this paper uses small explosive charges as sources to generate interface waves and the

DREA ocean bottom seismometer (OBS) as a receiver. Two sites on the Scotian Shelf with clay as the surficial sediment were selected for the experiment. To our knowledge, this is the first publication presenting shear speed profiles for the surficial sediments on the Scotian Shelf collected using this seismo-acoustic inversion technique. The interface waves generated in this experiment propagated at group velocities and frequencies which are among the lowest—if not the lowest—that have been reported in the literature [Snoek, 1990; Stoll *et al.*, 1994]. Using this technique, the shear speed of the approximately 40 m of clay and silt in the Quaternary succession on the Scotian Shelf is determined to vary from approximately 10 m/s at the seabed to 120 m/s at 40 m depth, increasing as a power-law function of depth with an exponent in the range of 0.60 to 0.65.

2. GEO-ACOUSTIC ENVIRONMENT OF EXPERIMENTAL SITES

The prominent physiographic features of the Scotian Shelf are shallow banks (~100 m depth) and deeper basins (150-300 m depth). The unconsolidated surficial sediments on the Scotian Shelf were deposited during the late Quaternary period (the last 25,000 years before present). The sediment types and their distribution are linked to two related events: the Wisconsinan Glaciation, the most recent episode of glaciation on the Scotian Shelf, which covered most of the Scotian Shelf with ice; and relative sea level changes, up to 115 m lower than present, which led to sub-aerial exposure of the shallower areas. On average, the thickness of the Quaternary succession is 50 m. Following King [1970], the lithostratigraphy for the banks is typically sand underlain by glacial till, while the basins have clay and silt overlying the glacial till. (The information and nomenclature of the following two paragraphs is also based on King [1970].)

The glacial till, "Scotian Shelf Drift Formation", is deposited from grounded ice. In water depths >120 m, it overlies much of the bedrock on the Scotian Shelf in the sub-surface as a continuous blanket of relatively uniform thickness (10–15 m). It is a cohesive poorly sorted sediment generally containing angular fragments in the pebble / cobble / boulder range. It is dominantly sandy but contains abundant silt and clay. (This formation is found in water depths up to 260 m, but its maximum extent is not known.) The "Emerald Silt Formation" overlies and interfingers with the Scotian Shelf Drift. While similar in composition to the Scotian Shelf Drift, it was formed from subglacial meltout debris from a stable but floating ice shelf. The stratigraphy has a banded nature because of the differential sorting of material settling through the water column. Accordingly, there is a strong contrast in the acoustic character of the two formations which serves a basis to distinguish them. The "Sable Island Sand and Gravel Formation" is comprised of well-sorted and well rounded sand and gravel particles. It is
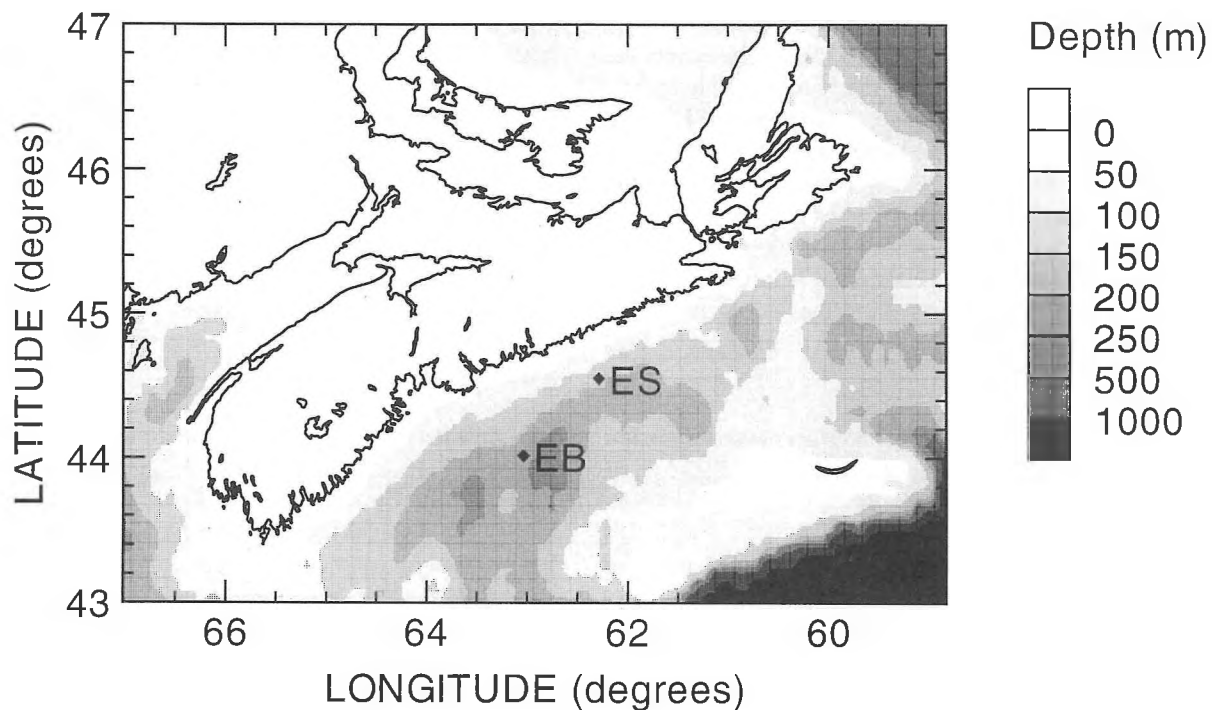
Figure 1: Bathymetry of the Scotian Shelf and locations of interface wave dispersion experiments. EB=Emerald Basin, ES=Eastern Shore.
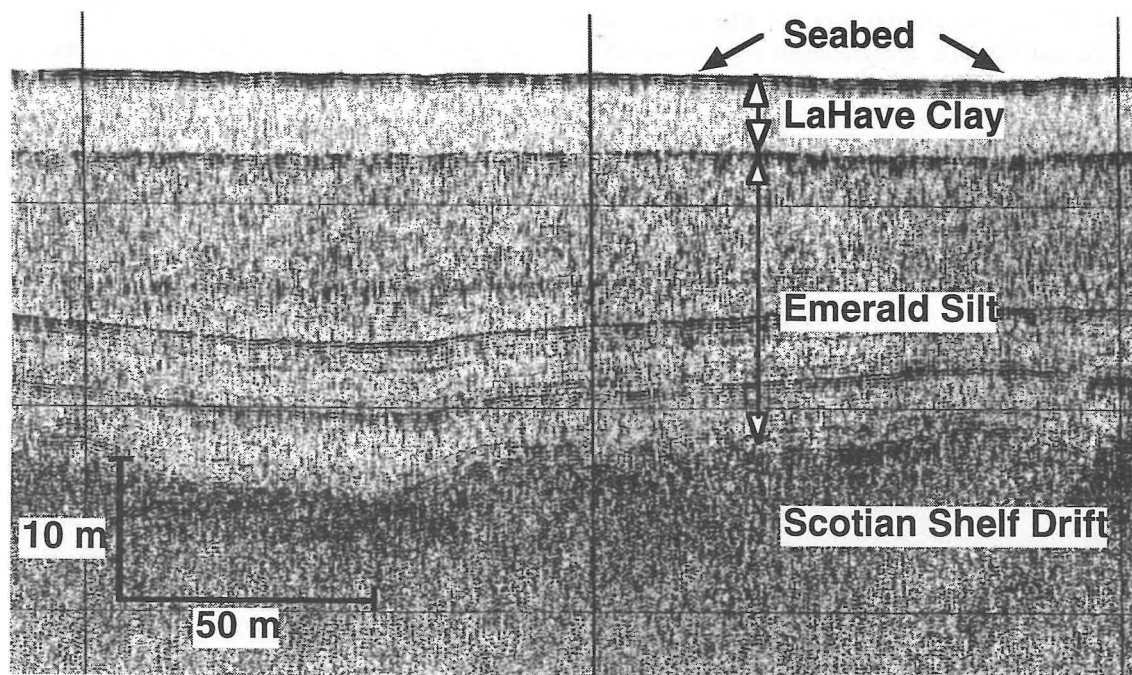

Figure 2: Seismic reflection profile of the Quaternary succession at the ES site obtained with a 3.5 kHz profiler towed approximately 20 m above the seabed [Canadian Seabed Research, Ltd., 1996].

mainly derived from the erosion of former glacial deposits on the shallow banks. These sediments, above the lowest sea level stand (120 m), were reworked in the high energy environment present when relative sea-level was rising. The "LaHave Clay" is a postglacial loosely compacted silty clay to clayey silt. It was deposited at the same time as the Sable Island Sand and Gravel and its distribution is mainly confined to the basins and depressions of the shelf where it is ponded over underlying sediments. It is derived by a winnowing of the fine material from the sediments on the banks during relative sea level rise and from adjacent land areas.

The two experimental sites for the interface wave dispersion studies are marked in Fig. 1. They are located in northwestern Emerald Basin (EB) at 44°0.792' N, 63°1.308' W and seaward of the Eastern Shore (ES) area of Nova Scotia at 44°32.826' N, 63°17.400' W. At both sites, the surficial sediment type is LaHave Clay, underlain by Emerald Silt and then Scotian Shelf Drift. The EB site was chosen [Osler, 1994] because of the availability of a wide diameter geotechnical core and seismic reflection and refraction profiles using Huntec "boomer" [Moran *et al.*, 1991; Courtney, 1996, Personal Communication], airgun [Louden, 1994], and 3.5 kHz piezoelectric [Canadian Seabed Research, Ltd., 1996] sources. The OBS was deployed in 219 m of water, over 9 m of LaHave Clay, and 29 m of Emerald Silt. The geotechnical core, 87003-002 [Courtney and Mayer, 1993], has a 17 m penetration with measurements of compressional-wave speed, bulk density, water content, grain size, shear strength, impedance, magnetic susceptibility, and compressional-wave attenuation at 500 kHz. The median grain size in the core is

2 µm, porosities range from 80% at the seabed to 55% at the base of the core, and bulk densities are approximately 1500 kg/m³ for LaHave Clay and 1600 kg/m³ for Emerald Silt. The compressional-wave speed measured in the core is 1.45 to 1.49 km/s, consistent with field measurements of 1.46 to 1.49 km/s for LaHave Clay [Dodds, 1990]. Even though the clay is considered "rigid" (i.e. the shear modulus is non-zero), the compressional-wave speed of the surficial sediment is less than the typical speed of sound for bottom waters at this site, as the compressibility does not increase as rapidly as the bulk density in moving from the water into the sediment.

The ES site is situated in 156 m of water with a seabed comprised of 5.5 m of LaHave Clay overlying 20 m of Emerald Silt. The reflection profile (Fig. 2) is similar to that at the EB, however the boundary between the rhythmically banded Emerald Silt and the underlying Scotian Shelf Drift is more readily discerned. While there is limited geotechnical information at the ES site (surficial grabs and cores with 1 m penetration), the similarity in the reflection profiles and identification of the LaHave Clay and Emerald Silt formations suggests that the geo-acoustic environment is similar to that at EB. An exception may be the possibility of trapped gas within the surficial sediments [Moran *et al.*, 1991; Fader, 1991] at the EB site. Sidescan sonar images at the EB site [Canadian Seabed Research, Ltd., 1996] reveal that gas escape craters "pockmarks" are abundant while no evidence for pockmarks was seen in sidescan sonar images at the ES site.

3. OBS DESIGN AND INTERACTION WITH THE SEABED

The Acoustic Sensor Module of the DREA OBS (Fig. 3) houses the geophone sensors. It was built under contract according to DREA specifications [Dodds, 1994; Dodds *et al.*, 1994]. It consists of an orthogonal triad of 4.5 Hz geophones mounted on a block which is leveled and clamped to the base of the 0.25 m diameter spherical glass pressure vessel once the OBS has been deployed on the seabed. The pressure vessel is clamped to an aluminum coupling disk, formed by two concentric 0.66 m diameter horizontal plates connected by a framework of rods. This design provides a coupling disk which is rigid below 50 Hz, while keeping its mass minimal. The ASM is connected to a deployment frame by ropes which slacken when the OBS is on the seabed to decouple the ASM from the frame. The frame houses the deployment and recovery gear, power supply and telemetry electronics, protects the ASM during deployment and recovery, and provides a terminus for the armoured cable that carries the signals to the surface float (Fig. 5).
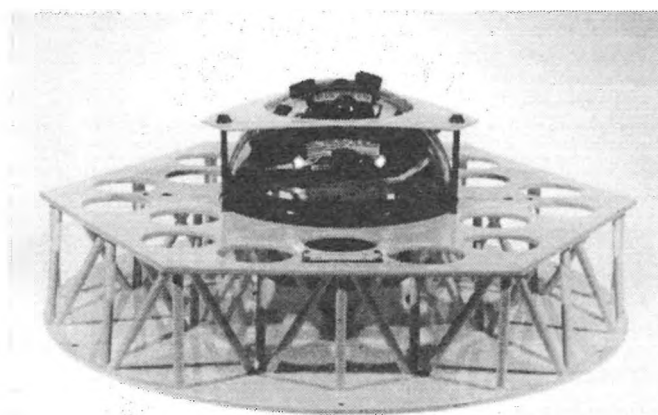

Figure 3: The Acoustic Sensor Module of the DREA Ocean Bottom Seismometer. The sphere housing the geophones has a diameter of 0.25 m and is clamped to the 0.66 m diameter coupling disk.
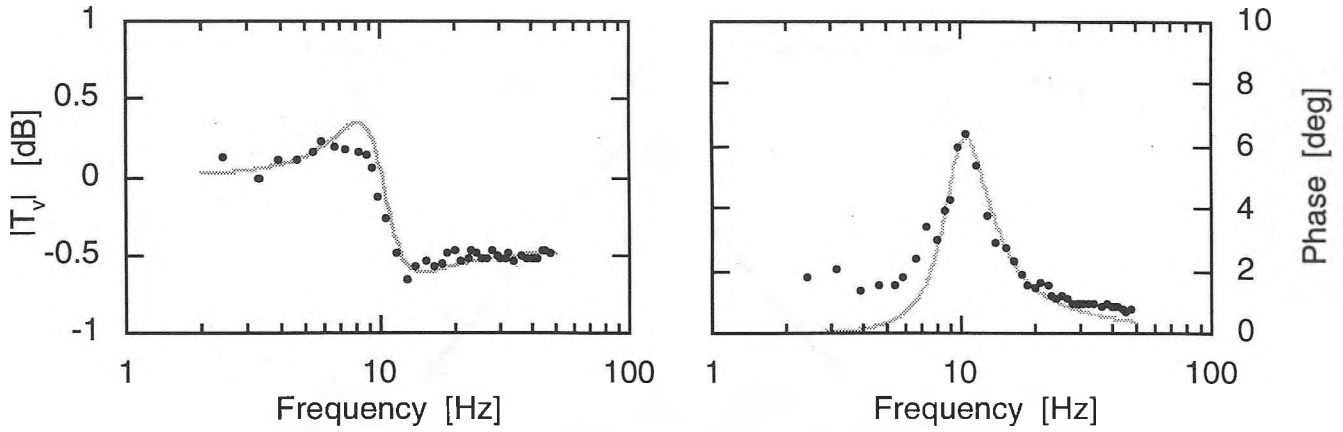
Figure 4:   The vertical motion seabed/OBS transfer function for a typical deployment on a clay seabed. The data points are values directly calculated from the measurement; the smooth curves are based on a mass-spring-dashpot model.

The ASM is designed to minimize the interaction effects with the seabed [Dodds *et al.*, 1994] following the recommendations made by Sutton and Duennebier [1987]. Osler *et al.* [1994] derived transfer functions for the interaction of an OBS with the seabed and then applied this theory to experiments using the DREA OBS. By transfer function, we mean the ratio of the actual OBS velocity to the velocity of the seabed upon which the instrument rests, i.e. the actual quantity of interest. For faithful measurement, the transfer function should be as close to unity as possible. (Our analysis applies to any OBS for which rocking effects and interaction with nearby instrument packages can be ignored.) The transfer function for motion of the OBS in response to vertical seabed motion is

$$T_v = 1 - \frac{r}{r_\infty}\left(\frac{m - m_w}{m + m_{bot}}\right) \tag{1}$$

where r is the frequency-dependent "coupling ratio", m_{bot} is the hydrodynamic added mass of the OBS when it is on the seabed, m is the inertial mass of the OBS, m_w is the mass of water it displaces, and

$$r_\infty = \frac{m + m_{sus}}{m + m_{bot}}, \tag{2}$$

where m_{sus} is the hydrodynamic added mass of the OBS when it is freely suspended in water. The coupling ratio is the ratio of the response of the ASM to forced motion when it is freely suspended in water and when it is on the seabed. The forcing at different frequencies in its 1–50 Hz operating band is effected by a miniature DC motor mounted inside the pressure vessel driving an eccentric mass of about one gram located about one-half centimetre off-axis. The excitation has both vertical and horizontal components and the phase of the forcing is tracked by a photo-optic sensor which detects the passage of the eccentric mass through a reference point.

When both amplitude and phase of the coupling ratio data are measured, the transfer function can be calculated directly by substituting the measured coupling ratio data into Eq. (1). The transfer function for a typical deployment on clay is shown in Fig. 4. The vertical transfer function is within 0.75 dB of unity at all frequencies, by virtue of the large hydrodynamic added mass, m_{bot}, which the coupling disk provides in the vertical (Fig. 3). We regard this correction to be insignificant for the purpose at hand, and we did not apply it to the data. The phase responses show some scatter, but only at very small phase values or when the magnitude response is very small. The measurement of seabed/OBS coupling indicates that the interface wave dispersion data (to be presented next) are accurate renderings of the true seabed motion.

4.   EXPERIMENTAL PROCEDURE

Interface waves on the water-sediment boundary were generated by detonating small explosive charges at or near the seabed. The charges were formed with C4 plastic explosive molded around a blasting cap (non-electric No. 12) crimped to a fuse (M700) of sufficient length to burn for approximately 4 minutes. The charges were sealed in plastic, weighted to ensure they would descend to the seabed, and then deployed at different horizontal ranges as *C.F.A.V. Quest* proceeded away from the OBS at approximately 4 knots. Signals received on the DREA OBS geophones and hydrophone were digitized in the OBS, telemetered to *C.F.A.V. Quest* via the surface float, processed and displayed in real time to monitor data quality, and recorded for subsequent analysis (Fig. 5). Several measures were taken to mitigate the potential environmental impact of the explosions. Different charge weights from 100 to 500 g were tested during an initial experiment. The 250 g charges were the smallest with sufficient low frequency energy to generate interface waves on the soft clay seabed. As they were only effective at ranges less than approximately 300 m and had less energy in the higher order
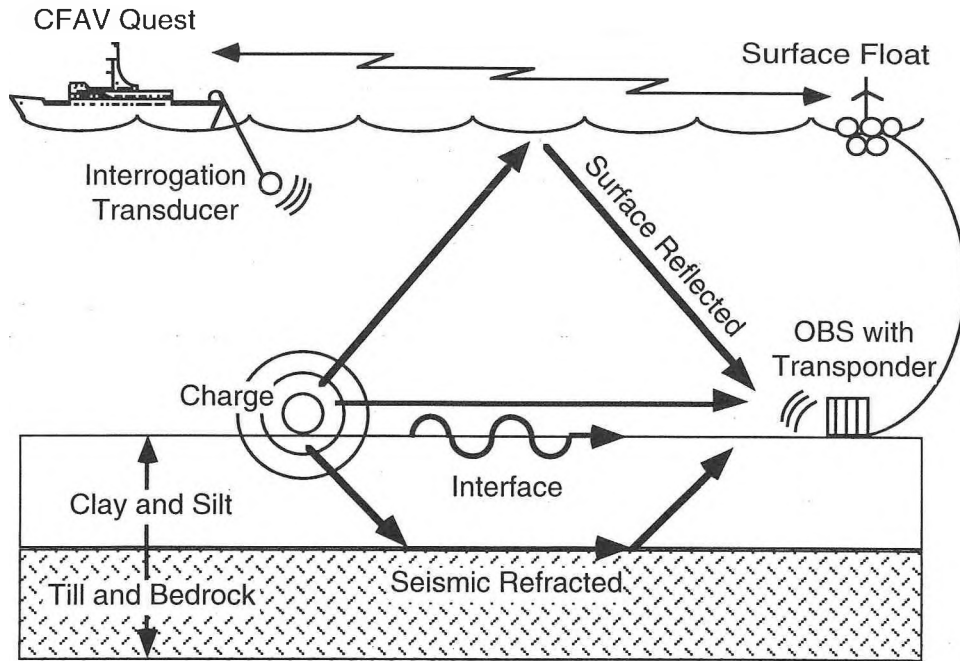
Figure 5:   Source to receiver arrival paths and schematic of experimental setup.

modes (crucial in constraining models of shear speed structure), the 500 g charges were favoured. During the experiments, sonobuoys were deployed to listen for marine mammal vocalizations, the ships echo sounder was monitored for reflections from schools of fish, and the bridge maintained a visual watch for mammals on the surface.

Precise navigation was essential for the safe and successful conduct of this experiment. The ship itself uses Global Positioning System (GPS) navigation, whose inaccuracies may introduce errors of up to 100 m in absolute position. The OBS deployment frame was fitted with an acoustic transponder to measure the slant range to an interrogating

transducer towed astern of *C.F.A.V. Quest* (Fig. 5). Prior to deploying explosives, the absolute position of the instrument was found [FITDS software, D.J. Dodds, GeoAcoustics Inc.] by minimizing the summed squared deviation between "observed" and "calculated" travel times using the Levenberg-Marquardt method [Dennis and Schnabel, 1983; Moré, 1977]. The observed travel time is that measured by the transponder system. The calculated travel time is that between the known interrogator position and an estimated position for the transponder—specified for the initial calculation and then revised to minimize the summed squared deviation. Typically 200 to 400 range measurements were used for each position determination. The calculated travel times are made assuming a reasonable
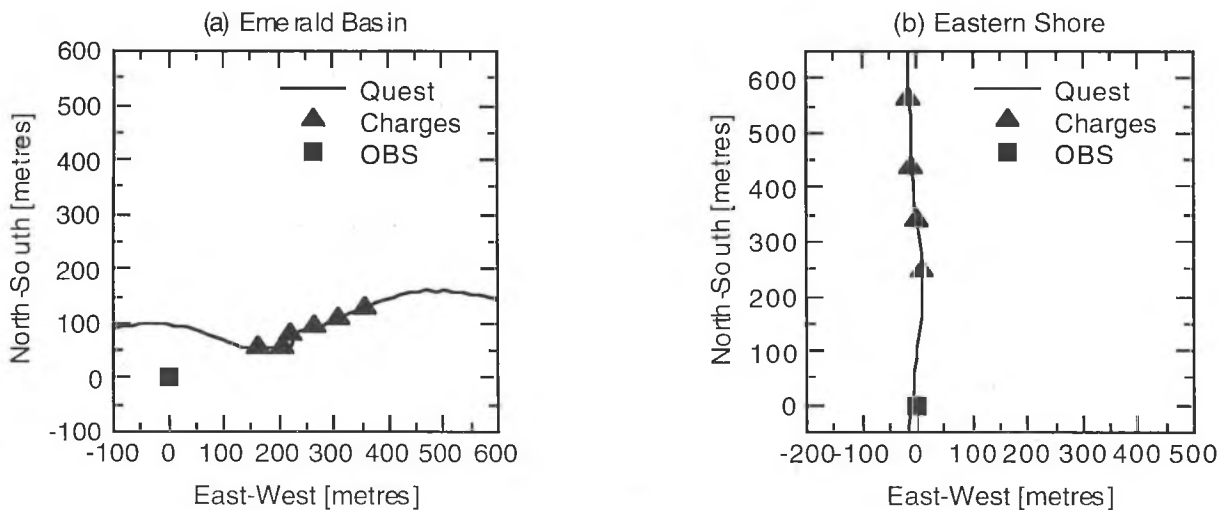

Figure 6:   Geometry of interface wave dispersion experiments at (a) the EB and (b) the ES site. Charge drop positions are GPS-derived positions and may not agree with acoustic ranges derived using Eq. 3.

speed of sound, but it can also be a variable in the minimization. During an experiment, the slant and horizontal range of *C.F.A.V. Quest* relative to the OBS was monitored and once the OBS had been safely transited, charges were dropped at specified time or range intervals. The accuracy of relative range measurements is estimated at 5 m, limited by uncertainty in the position of the interrogating tow fish. Using this method, the scatter due to GPS error can be reduced, although there may still remain a bias in the resulting absolute position.

Plan views of the geometry of the experiments at the Emerald Basin and Eastern Shore sites are displayed in Fig. 6. The track of *C.F.A.V. Quest* and the drop positions of the charges are plotted relative to the absolute position of the OBS. Because the charges may drift laterally while descending to the seabed, accurate source to receiver ranges, l, were calculated using

$$l = \frac{c^2 \Delta t^2 - 4d^2}{2c\,\Delta t},\qquad(3)$$

where Δt is the difference in travel time between the direct and surface reflected arrival paths, c is the speed of sound in water and d is the water depth.

Sound speed profiles were measured with expendable sound velocimeters (XSVs), but precise details of the sound speed have little effect on the analysis, and a representative value of 1490 m/s has been used throughout. In particular, the transponder-positioning algorithm gives good results even if the assumed sound speed is not accurate, and the group speed of the interface wave modes (to be discussed below) is insensitive to the sound speed profile.

5. RESULTS

At each site, the interface wave generated at the shortest range—100 m for EB and 224 m for ES —has been selected for the dispersion analysis. The time series of vertical seabed motion as sensed by the geophones are plotted in the right panel of Figs. 7a and 7b, for EB and ES respectively.

To reduce the dynamic range of the display, the amplitude of the time series has been compressed by a square root scaling factor. (This somewhat unconventional compression portrays the energy distribution in the waveform without distorting signals as much as a logarithmic compression.) The direct arrival is not shown because of the large disparity between the level of the interface wave and the direct arrival. The slowly propagating interface wave arrives at the OBS from 2 to 11 seconds after the direct water borne arrival at EB and from 5 to 15 seconds at ES.

The left panels in Figs. 7a and 7b are time-frequency-intensity decompositions of their respective interface waves displayed in the right panel. As with the time series, the amplitude of the power spectral density has been reduced by a square root compression before contouring to enhance the energy in lower amplitude arrivals (*e.g.* the higher order modes). The image of power spectral density was calculated using the *S* transform [Stockwell *et al.*, 1996] which is a joint time-frequency representation analysis technique with a frequency-dependent resolution. It is an extension of the Gabor [1946] and Wavelet [Goupillaud *et al.*, 1984] transforms designed to extend the principles of Fourier analysis to non-stationary time series. For a gaussian window width proportional to the period of the sinusoid being localized, as used to prepare Fig. 7, the *S* transform is

$$S(f,\tau) = \frac{1}{\sqrt{2\pi}} \int_{-\infty}^{\infty} h(t)|f| e^{-(\tau-t)^2 f^2/2} e^{i2\pi f t} dt,\qquad(4)$$

where τ is the translation parameter with the same dimension as time, $h(t)$ is the time series, and f is frequency.

The vertical axes for the images in Fig. 7 represent group speed, calculated using the time of flight since detonation of the charge and the source-receiver ranges calculated as previously specified. At each site, two interface wave modes are localized by the transform: a fundamental mode spanning 1 to 3 Hz having a group speed ranging from 10 to 40 m/s at EB and 15 to 50 m/s at ES; and a second mode

Table 1: Geo-acoustic Parameters for Interface Wave Dispersion Modelling

	water	clay	silt	till
density (normalized)	1	1.5	1.6	2.0
compressional-wave speed [m/s]	1490	1450	1550	1800
shear-wave speed [m/s]	-	(see Fig. 9)	(see Fig. 9)	180
compressional-wave attenuation [dB/λ]	-	0.2	0.5	0.5
shear-wave attenuation [dB/λ]	-	1.0	1.5	1.0
layer thickness at EB [m]	∞	9	29	∞
layer thickness at ES [m]	∞	5.5	20	∞

spanning 2.5 to 4 Hz having a group speed ranging from 15 to 30 m/s at EB and 25 to 35 m/s at ES. The group speed of an interface wave is related to the shear speed in the seabed to a depth of 1 or 2 wavelengths [Stoll *et al.*, 1991]. Interface waves have a dispersive nature—the lower frequency components penetrate deeper into the seabed where higher speed material is encountered. Consequently, they propagate at a higher group speed and arrive earlier at the OBS than the higher frequency components. (Note that the vertical axis for theses figures is actually linear in time, allowing grey-scale features to be identified with time-series features; however, the corresponding group speed has been indicated as an additional non-linear scale on the gry-scale plot.)

We modelled the dispersion of the interface wave modes using the pulse version of the SAFARI fast-field seismo-acoustic propagation model [Schmidt, 1988] which has an option to calculate curves of phase and group speed vs. frequency for a specified environment. Dosso and Brooke

[1995] used this technique for their data and found that the results were extremely sensitive to the profile of shear speed vs. depth in the seabed, and much less sensitive to the other seismo-acoustic parameters, such as compressional wave speed, layer densities, attenuations, etc. Our model consists of a water half-space above, a clay layer, a silt layer, and a till half space below; the numerical values for the geo-acoustic inputs are shown in Table 1, except for the shear speed profile. The layer thicknesses were derived from vertical-incidence seismic reflection profiles at the sites (*e.g.* Fig. 2) gathered during a contracted survey [Canadian Seabed Research, Ltd., 1996].

SAFARI treats the seabed as a sequence of parallel layers of elastic solid, each layer having constant properties. If a quantity is thought to have a continuous gradient with depth—as in the case of the shear speed for soft sediments—then it is necessary to divide a material layer into several sub-layers, approximating the continuous profile with a staircase-like piecewise constant sequence.
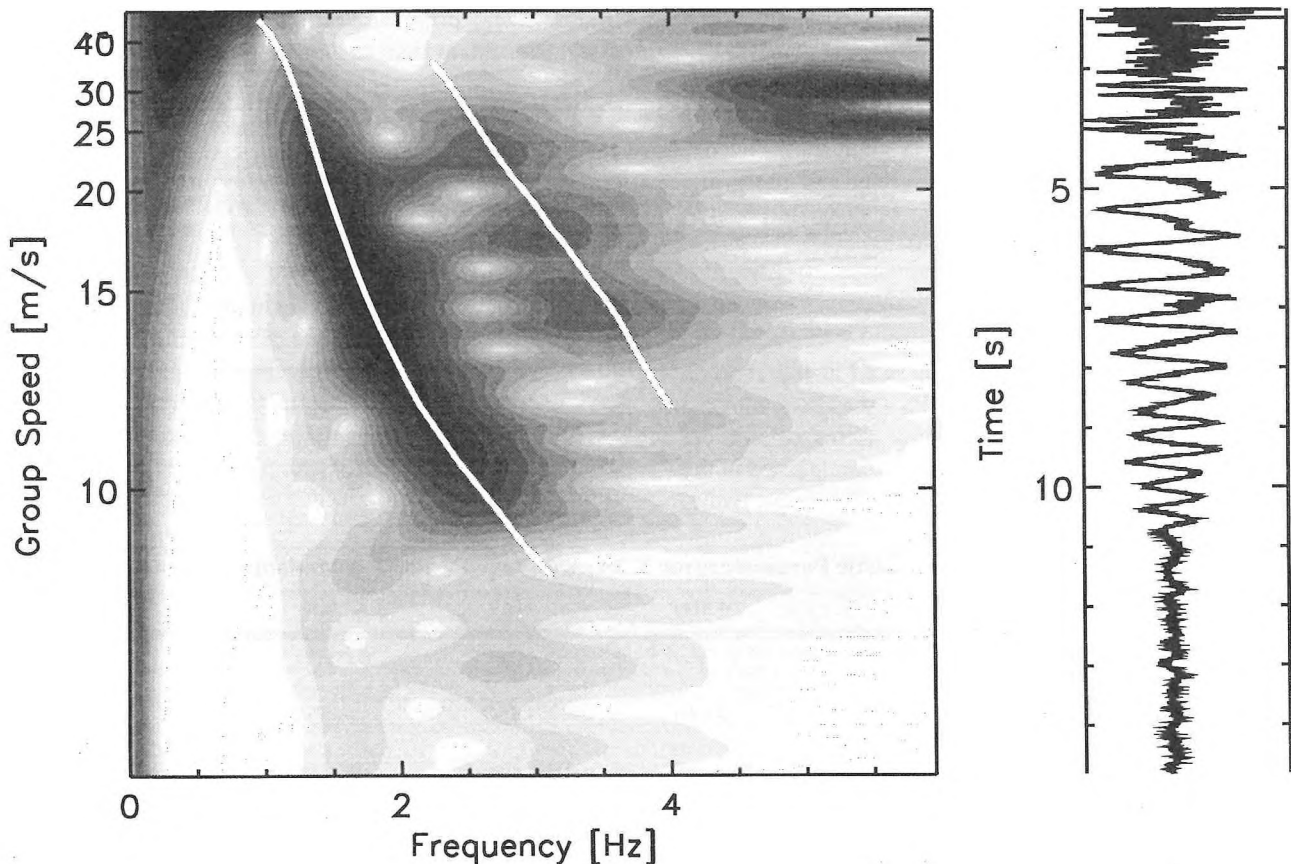

Figure 7(a)   S transform of an interface wave at the EB site (right hand panel). Solid line is the dispersion curve calculated using SAFARI and the shear-wave speed profile (Fig. 9). Square-root dynamic compression has been applied to both time series and grey scale to emphasize low-level signals.

The observed dispersion data suggest that lower-frequency waves travel faster, implying that the longer wavelengths penetrate deeper and sample higher-speed material. (Dispersion could also result from the waterborne portion of the interface wave sensing the upper boundary of the ocean [Ewing et al., 1957], but this effect occurs at frequencies much lower than our measurements, due to the very low wave speeds involved.) Following the suggestion of Stoll et al. [1991], we generated shear-speed staircases from an assumed continuous power-law profile of the form

$$c_s(z) = c_0 z^\nu , \qquad (5)$$

in which c_s is the shear speed at depth z and c_0 and ν are parameters that control the shape of the profile. Because the shear speed (and hence the wavelength) increases with depth, we made each successive sub-layer progressively thicker to approximately maintain the same thickness-to-wavelength ratio for all the sub-layers. We used 11 clay and silt layers at EB and 9 layers at ES, where the soft sediments were not as thick. The resulting clay and silt sub-layer boundary depth sequence (in metres) is $z_n = \{0, 0.25, 0.5,$ 1.5, 3.0, 5.5, 9.0, 13.5, 19.5, 25.5, 32, 38\}. Then we calculated the sub-layer shear speeds from the formula

$$c_n = (1 - \nu)c_0(z_{n+1} - z_n)/(z_{n+1}^{1-\nu} - z_n^{1-\nu}) , \qquad (6)$$

which is derived from the principle that the travel time through a homogeneous sub-layer should be the same as the travel time through the same depth interval calculated using the continuous gradient of Eq. (5).

The inversion of the interface wave dispersion data to obtain the shear speed structures is accomplished through forward iterative modelling. Using reasonable guesses for the parameters c_0 and ν, we calculate starting values for the shear speed staircase from Eq. (6) and include them with the parameters in Table 1 to prepare a SAFARI input file. After running the model, we compare the calculated group speed curves with the measured dispersion data. To simplify the comparison, we pick the maximum energy points from the time-frequency-intensity plots in Fig. 7 and plot them as speed-frequency plots along with the modelled group speed curves, as shown in Fig. 8. (The uncertainty in the
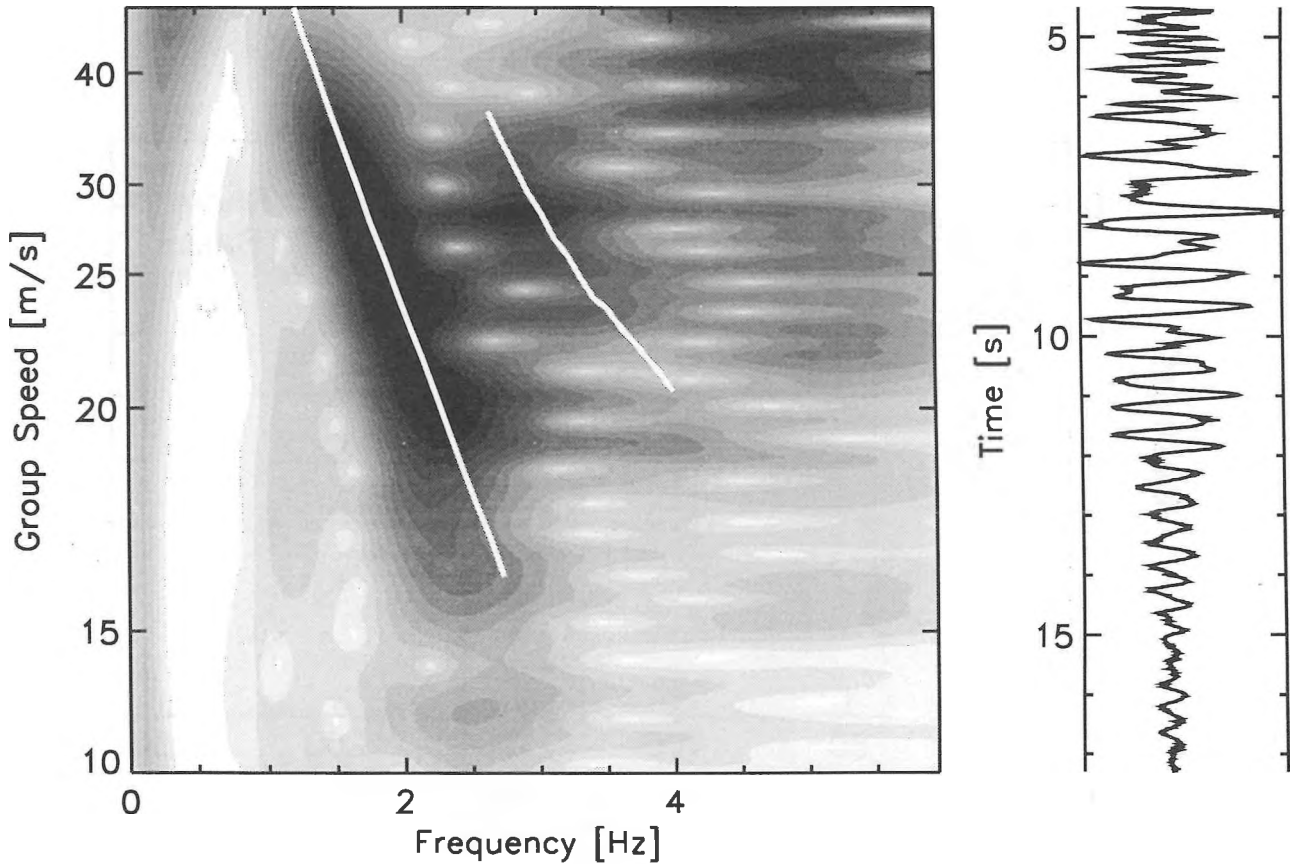

Figure 7(b): S transform of an interface wave at the ES site (right hand panel). Solid line is the dispersion curve calculated using SAFARI and the shear-wave speed profile (Fig. 9). Square-root dynamic compression has been applied to both time series and grey scale to emphasize low-level signals.
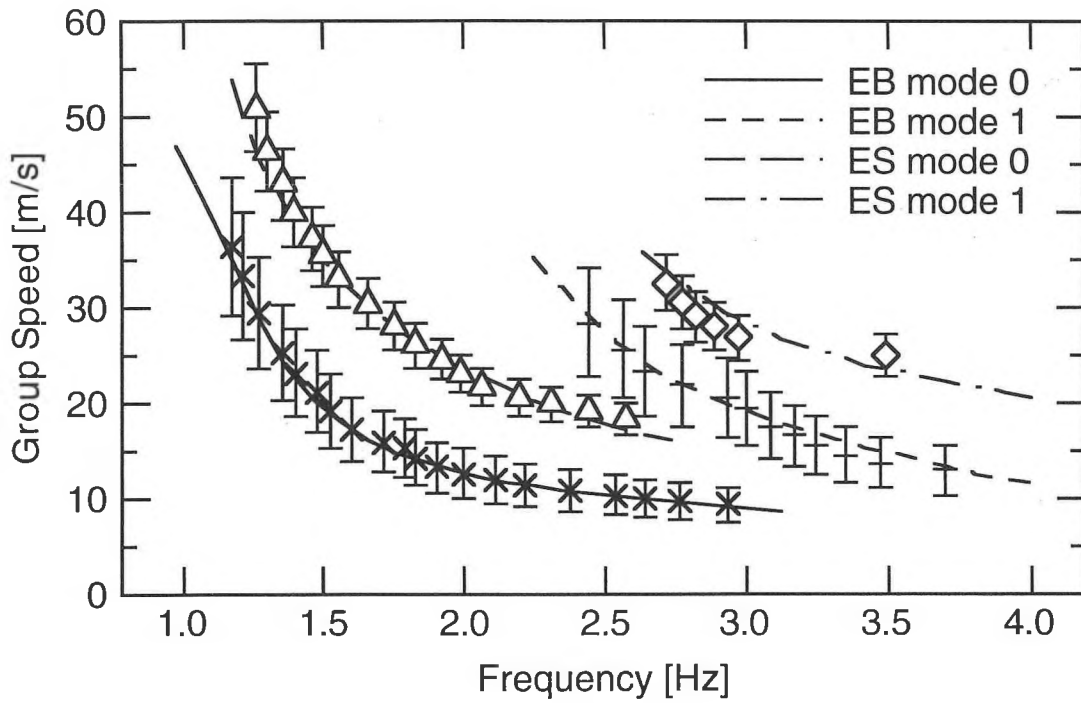
Figure 8: Picks of maximum energy for the fundamental and higher order modes at the EB and ES sites are fit by theoretical dispersion curves calculated using SAFARI and the shear-wave speed profile in Fig. 9.
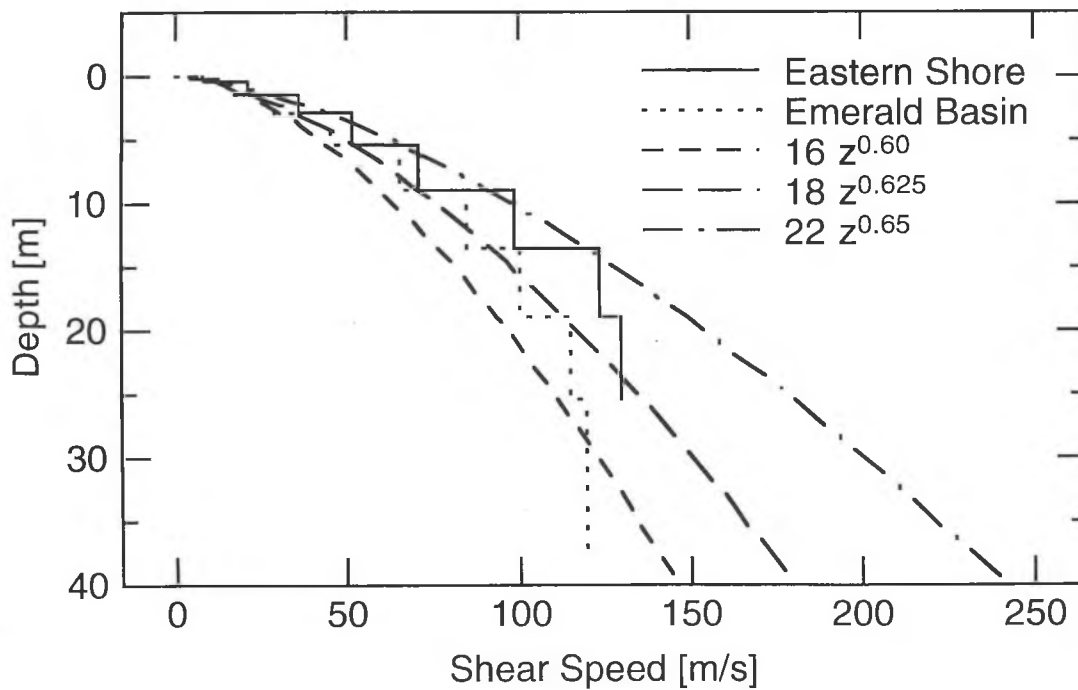

Figure 9: Shear-wave speed from the inversion of interface wave dispersion data at the EB and ES sites on the Scotian Shelf.

measured speeds derives from an uncertainty of ± 20 m in the calculated source-receiver ranges.) We vary the parameters c_0 and v systematically and run SAFARI several times to achieve a reasonable fit overall, then we abandon Eq. (6) and adjust sub-layer shear speed values individually to obtain the final fit such as in Fig. 8. (We expect that actual sediment deposition processes would result in some variation of shear speed away from a smooth profile.) The resulting shear speed profiles for the EB and ES sites are shown in Fig. 9, along with some power-law profiles for comparison. The best-fit staircases are approximated by power law profiles with parameters $v = 0.63 \pm 0.03$ and $c_0 = 18.5 \pm 0.5$ m/s re 1 m for the EB site, and $v = 0.60 \pm 0.02$ and $c_0 = 21.5 \pm 0.5$ m/s re 1 m for the ES Site. The modelled dispersion curves are also superimposed on the grey-scale representations of the interface waves (Figs. 7a and 7b respectively).

Although the resulting profiles in Fig. 8 are plausible, there is some doubt regarding their uniqueness, as other workers have pointed out that the influence of the deeper layers becomes progressively less due to the concentration of energy in the interface wave modes towards the upper boundary. In this regard, at a given frequency, the higher-order modes seem to sample deeper sub-layers than the fundamental mode. Finding shear speed profiles to fit the dispersion of the fundamental mode is relatively easy, but inclusion of the higher mode in the fit restricts the range of allowed profiles. To refine the fit, more data would be required, perhaps from sources at different ranges or having more energy to excite higher modes in deeper layers. In summary, more confidence should be placed in the upper layers of these fits than in the lower.

6. DISCUSSION

Using an ocean bottom seismometer designed and partially constructed by DREA—the construction of the sensor portion having been contracted out—we have successfully recorded and interpreted explosively-generated interface waves on the seabed at two sites whose uppermost sediments are classified as clay and silt. Inversion of the measured dispersion data (*i.e.* group speed vs. frequency) using repetitive forward modelling with the SAFARI code has produced plausible profiles of shear speed vs. depth that are consistent with approximate power-law shear profiles of the form $c_s(z) = c_0 z^v$, with v in the range 0.60–0.65 and c_0 in the range 16-22 m/s re 1 m. These measurements appear to be the first of their kind on the eastern Canadian continental shelf and the shear speeds fitted for the uppermost sub-layers are among the lowest determined anywhere using this method.

The fitted exponent v seems higher than those for other sediments, which are of the order 0.3 [Stoll *et al.*, 1991].

(The uncertainty in source-receiver range translates into a proportional uncertainty in the c_0 parameter, but has little effect on the fit for the exponent v.) This deserves further investigation, particularly concerning the role of porosity in determining the shear speed. The Stoll *et al.* study assumes porosity is constant with increasing depth, so a porosity gradient might explain the higher exponent for the shear speed profile in clay. It is interesting to note that despite the high porosities and small grain sizes which lead the LaHave Clay to be classified as a suspension (*i.e.* the pore-fluid is stress-bearing rather than the grains [Courtney and Mayer, 1993; Nur *et al.* 1991]), the ability to generate interface waves in the material reveals that it does have some rigidity. Our observations concerning the nature of this material may also be of some use to geotechnical projects, such as the burial of submarine cables.

This paper does not consider the effect of the observed shear speed profiles on acoustic conditions for sonar operation, but the information provides a basis for such a study to be performed. These measurements provide ground truth for ocean acoustic experiments planned for the same sites.

REFERENCES

Akal, T., 1980, Sea floor effects on shallow-water acoustic propagation, in Bottom-Interacting Ocean Acoustics, ed. Kuperman, W.A. and Jensen, F.B., NATO Conf. Ser. 4, 5, 557-575.

Ali, H.B., and Bibee, L. D., 1993, The influence of sediment layering and geoacoustics on the propagation of Scholte interface waves, in Proceedings of Oceans 93, IEEE, New York, 105-113.

Bennell, J. D., and Smith, D. T., 1991, A review of laboratory shear wave techniques and attenuation measurements with particular reference to the resonant column, in *Shear Waves in Marine Sediments*, eds. Hovem, J. M., Richardson, M.D., and Stoll, R.D., Kluwer Academic Publishers, 83-93.

Caiti, A., Akal, T., Stoll, R.D., 1993, Shear wave velocity in seafloor sediments by inversion of interface wave dispersion data, SACLANTCEN Report SR-205, 53 pp.

Canadian Seabed Research, Ltd., 1996, Seabed mapping for DREA experimental sites, DREA Contractor Report CR/96/404, 74 pp.

Chapman, D.M.F., Hughes, S.J., Staal, P.R., 1992, Shallow water acoustics: a review of DREA research, Canadian Acoustics, 20, 37-42.

Chapman, D.M.F., Osler, J.C., Risley, W.C., Dodds, J.C., 1994, Underwater acoustic measurements with a digital ocean bottom seismometer (Abstract), Journal of the Acoustical Society of America., 96, 3330.

Courtney, R. C., and Mayer, L. M., 1993, Acoustic properties of fine-grained sediments from Emerald Basin: Toward an inversion for physical properties using the Biot-Stoll model, Journal of the Acoustical Society of America., 93, 3193-3200.

Davis, A.M., Bennell, J. D., Huws, D.G., Thomas, D., 1989, Development of a seafloor geophysical sledge, Marine Geotechnology, 8, 99-109.

Dennis, J.E., and Schnabel, 1983, Numerical Methods for Unconstrained Optimization and Nonlinear Equations. Prentice-Hall, Eaglewood Cliffs, New Jersey, U.S.A.

Dodds, J., 1990, Seabed sound speed data analysis, DREA Contractor Report CR/90/404, 42 pp.

Dodds, D. J., 1995, Design study for sea-floor shear-wave source, DREA Contractor Report 95/451, 94 pp.

Dodds, D.J., Chapman, D.M.F., Osler, J.C., Risley, W.C., 1994, Minimizing instrument effects in an ocean bottom seismometer (Extended Abstract), Canadian Acoustics, 22, 161 - 162.

Dodds, 1994, Acoustic sensor module for deployment on the seabed, DREA Contractor Report 94/459, 53 pp.

Dosso, S. E., and Brooke, G. H., 1995, Measurement of seismo-acoustic ocean-bottom properties in the high Arctic, Journal of the Acoustical Society of America, 98, 1657-1666.

Ewing, W. Maurice, Jardetzky, Wenceslas S., and Press, Frank, 1957, *Elastic Waves in Layered Media,* Mcgraw-Hill, New York, p. 162.

Ewing, J., Carter, J. A., Sutton, G. H., Barstow, N., 1992, Shallow water sediment properties derived from high-frequency shear and interface waves, Journal of Geophysical Research, 97, 4739-4762.

Fader, G.B.J., 1991, Gas-related sedimentary features from the eastern Canadian continental shelf, Continental Shelf Research, 11, 1123-1153.

Gabor, D., 1946, Theory of Communication, Journal of the Institute of Electrical Engineering, 93, 429-457.

Goupillaud, P., Grossmann, A., and Morlet, J., 1984, Cycle-octave and related transforms in seismic analysis, Geoexploration 23, 85-102.

Hamilton, E.L., Bucker, H.P., Keir, D.L., and Whitney, J.A., 1970, Velocities of compressional and shear waves in marine sediments determined *in situ* from a research submersible, Journal of Geophysical Research, 75, 4039-4049.

King, L.H., 1970, Surficial Geology of the Halifax-Sable Island map area, Marine Science Paper 1, Department of Energy, Mines and Resources, Ottawa, Ontario, 16 pp.

Louden, K.E., 1994, The collection and anaylsis of seismo-acoustic data: Results from Dalhousie Ocean Bottom Seismograph recordings during CFAV Quest cruise Q211, DREA Contractor Report CR/94/416, 46 pp.

Moran, K., Courtney, R.C., Mayer, L.A., Miller, A.A., Zevenhuizen, J., 1991, Surficial geology and physical properties 12: central shelf: Emerald Basin, in: *East Coast Basin Atlas Series: Scotian Shelf*, AGC, Geological Survey of Canada, p. 133.

Moré, J.J., 1977, The Levenberg-Marquardt algorithm: implementation and theory, in: *Numerical Analysis*, Lecture Notes 630, ed. Watson, G.A., Springer Verlag.

Muir, T.G., Akal, T., Richardson, M.D., Stoll, R.D., Caiti, A., and Hovem, J. M., 1991, Comparison of techniques for shear wave velocity and attenuation measurements, in *Shear Waves in Marine Sediments*, eds. Hovem, J. M., Richardson, M.D., and Stoll, R.D., Kluwer Academic Publishers, 283-294.

Nur, A., Marion, D., Yin, H., 1991, Wave velocities in sediments, in *Shear Waves in Marine Sediments*, eds. Hovem, J. M., Richardson, M.D., and Stoll, R.D., Kluwer Academic Publishers, 131-140.

Osler, J.C., Chapman, D.M.F., Risley, W.C., Dodds, J.C., 1994, *In Situ* calibration of the coupling of an ocean bottom seismometer to Sand and Clay Surficial Sediments (Abstract), EOS transactions A.G.U. 75, 419.

Osler, J.C., 1994, A geo-acoustic and oceanographic description of several shallow water experimental sites on the Scotian Shelf, DREA Technical Memorandum 94/216, 45 pp.

Richardson, M. D., Muzi, E., Troiano, L., Miaschi, B., 1989, Sediment shear waves: A comparison of *in situ* and laboratory measurements, SACLANTCEN Memorandum SM-210, 21 pp.

Schmidt, H., 1988, SAFARI: Seismo-Acoustic Fast field Algorithm for Range-Independent environments, User's Guide, SACLANT Undersea Research Centre Report SR-11, 152 pp.

Snoek, M., 1990, Interface-wave propagation studies: An example of seismo-acoustic propagation in non-homogeneous materials, SACLANTCEN Memorandum SM-229, 33 pp.

Stockwell, R. G., Mansinha, L., Lowe, R. P., 1996, Localisation of the complex spectrum: The *S* transform, IEEE Signal Processing, 44(4), 998-1001.

Stoll, R. D., Bryan, G. M., Flood, R., Chayes, D., Manley, P., 1988, Shallow seismic experiments using shear waves, Journal of the Acoustical Society of America, 89, 2232-2240.

Stoll, R. D., Bryan, G. M., Mithal, R., Flood, R., 1991, Field experiments to study seafloor sesimoacoustic response, Journal of the Acoustical Society of America, 83, 93-101.

Stoll, R. D., Bautista, E., Flood, R., 1994, New tools for studying seafloor geotechnical and geoacoustic properties, Journal of the Acoustical Society of America., 96, 2937-2944.

Sutton, G.H., and F.K. Duennebier, 1987, Optimum design of ocean bottom seismometers, Marine Geophysical Research, 9, 47-65.